Title Page

Additive Manufacturing of Thermal Energy Storage Composites with Microencapsulated Phase Change Materials Supported in a Multi-Polymer Matrix

Kyle E. O. Foster*, Thomas B. Freeman, Irena Lizier-Zmudzinski, Susan Dudt, Karl B. Morgan, Sandra K. S. Boetcher, Adewale Odukomaiya*

Affiliations

Building Technologies and Science Center, National Renewable Energy Laboratory, 15013 Denver West Pkwy, Golden, CO 80401, USA

K. Foster kyle.foster@nrel.gov
T. Freeman thomas.freeman@nrel.gov,
I. Lizier-Zmudzinski lizierzmudzinski@mines.edu
S. Dudt srdudt@gmail.com
A. Odukomaiya adewale.odukomaiya@nrel.gov

Department of Mechanical Engineering, Embry-Riddle Aeronautical University, 1 Aerospace Boulevard, Daytona Beach, FL 32114, USA

T. Freeman thomas.freeman@nrel.gov
K. Morgan, morgak13@my.erau.edu
S. Boetcher boetches@erau.edu

Keywords

Thermal energy storage materials, thermal management, phase change materials, composites, advanced manufacturing, additive manufacturing, 3D printing

Abstract

Additive manufacturing (AM) techniques to directly integrate phase change materials (PCMs) are of interest for efficient thermal energy storage (TES) architectures. Complex, high surface-to-volume ratio composites embedded with PCM can improve thermal management with reduced material waste for customizable device fabrication. Reducing feature sizes of TES-integrated heat exchangers using AM can increase heat transfer without thermal conductivity enhancement. Here, composite AM materials containing 60wt.% microencapsulated-phase-change-materials (MEPCM) are fabricated using off-the-shelf printers at common speeds and resolutions. High MEPCM loading in filaments was achieved with powder extrusion using two polymers, thermoplastic-polyurethane (TPU) and polycaprolactone (PCL) that mediate flexibility and rigidity for effective extrusion and printing without filament fracture or buckling. With PCL and TPU at 20wt.% each and 60wt.% MEPCM ($P_{20}T_{20}M_{60}$), smooth, form-stable filaments are consistently printed. Powder-based extrusion displays negligible damaging effects on the MEPCM. Printed $P_{20}T_{20}M_{60}$ demonstrates 105 J/g of energy storage with no degradation through 250 thermal cycles, within 5% of the theoretical storage enthalpy. Combining PCL/TPU shows good interfacial adhesion between print layers and can produce high surface area objects, like 15% gyroids, and dense, 100% infilled pucks. Prints are also scalable to a 900 cm^3 honeycomb heat exchanger with an estimated 9 Wh energy storage.

Funding Statement

This work was co-authored by the National Renewable Energy Laboratory, operated by Alliance for Sustainable Energy, LLC, for the U.S. Department of Energy (DOE) under Contract No. DE-AC36-08GO28308. Funding provided by the U.S. Department of Energy Office of Energy Efficiency and Renewable Energy Building Technologies Office and the Advanced Manufacturing Office.

Conflict of Interest

The authors declare no conflict of interest.

Data Availability Statement

Data available within the article or its supplementary materials.

Table of Contents

Additive manufacturing of phase change materials (PCMs) can enhance thermal management of energy systems due to small length scales. Here, composite filaments with 60 wt.% PCM were developed, and 3D printed like typical commercial filaments. Advancements in processability and thermal energy storage were from powder mixing and extrusion of PCM with a multi-polymer matrix that balanced physical properties of filaments.

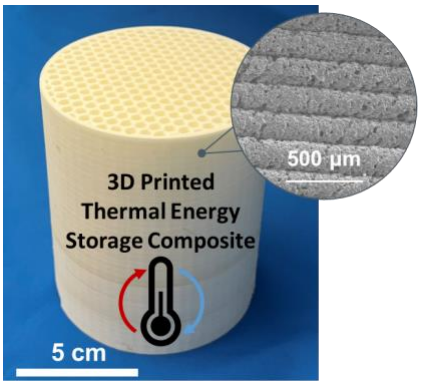

Highlights

- Improved phase change material capacity (60 wt.%) in filaments compared to previous technology
- Developed a stable MEPCM-filament extrusion process with negligible energy storage losses
- Printed diverse geometries, sizes (900 cm^3) at speeds/resolutions akin to commercial filaments
- Stable thermal transitions over hundreds of cycles
- Mechanically stable materials to withstand external strains from fluid flow and pressure changes

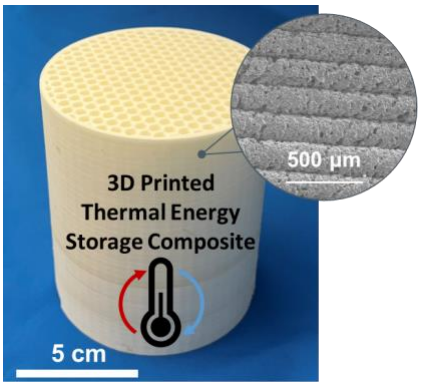

Additive Manufacturing of Thermal Energy Storage Composites with Microencapsulated Phase Change Materials Supported in a Multi-Polymer Matrix

Kyle E. O. Foster [a]*, Thomas B. Freeman [a,b], Irena Lizier-Zmudzinski [a], Susan Dudt [a], Karl B. Morgan [b], Sandra K. S. Boetcher [b], Adewale Odukomaiya [a]*

[a] Building Technologies and Science Center, National Renewable Energy Laboratory, 15013 Denver West Pkwy, Golden, CO 80401, USA

[b] Department of Mechanical Engineering, Embry-Riddle Aeronautical University, 1 Aerospace Boulevard, Daytona Beach, FL 32114, USA

*Corresponding Author: kyle.foster@nrel.gov, Adewale.Odukomaiya@nrel.gov

KEYWORDS

Thermal energy storage materials, thermal management, phase change materials, composites, advanced manufacturing, additive manufacturing, 3D printing

ABSTRACT

Additive manufacturing (AM) techniques to directly integrate phase change materials (PCMs) are of interest for efficient thermal energy storage (TES) architectures. Complex, high surface-to-volume ratio composites embedded with PCM can improve thermal management with reduced material waste for customizable device fabrication. Reducing feature sizes of TES-integrated heat exchangers using AM can increase heat transfer without thermal conductivity enhancement. Here, composite AM materials containing 60wt.% microencapsulated-phase-change-materials (MEPCM) are fabricated using off-the-shelf printers at common speeds and resolutions. High MEPCM loading in filaments was achieved with powder extrusion using two polymers, thermoplastic-polyurethane (TPU) and polycaprolactone (PCL) that mediate flexibility and rigidity for effective extrusion and printing without filament fracture or buckling. With PCL and TPU at 20wt.% each and 60wt.% MEPCM ($P_{20}T_{20}M_{60}$), smooth, form-stable filaments are consistently printed. Powder-based extrusion displays negligible damaging effects on the MEPCM. Printed $P_{20}T_{20}M_{60}$ demonstrates 105 J/g of energy storage with no degradation through 250 thermal cycles, within 5% of the theoretical storage enthalpy. Combining PCL/TPU shows good interfacial adhesion between print layers and can produce high surface area objects, like 15% gyroids, and dense, 100% infilled pucks. Prints are also scalable to a 900 cm^3 honeycomb heat exchanger with an estimated 9 Wh energy storage.

1 INTRODUCTION

Thermal energy storage is a key technology that can improve energy resiliency in many applications through thermal management and energy load shifting. Buildings in particular account for 76% of electricity usage and consume 40% of primary energy produced in the United States, which present an urgent challenge for achieving energy efficiency targets.[1] To address this issue, researchers have turned their attention to thermal energy storage (TES) systems as a cost-effective and long-lasting solution where phase change materials (PCMs), particularly solid-liquid PCMs, have attracted significant interest due to their energy storage capabilities.[2–4] Integration of PCMs into building TES systems can be achieved in passive and dynamic applications, with the potential to reduce daily indoor temperature fluctuations[5–7] and shift energy loads in HVAC and water heating systems.[8–12]

Some applications for PCMs in TES systems require high thermal energy density in a compact form that is difficult or expensive to manufacture with traditional methods and are still limited by effective charging and discharging with bulk forms of the PCM. Additive manufacturing (AM) can allow for production of compact heat exchangers with high surface areas that reduce heat transfer length scales to achieve more efficient heat transport.[8] Efforts to increase the thermal conductivity of AM materials with conductive additives have had limited success at the expense of material flexibility,[13] however there has been efforts to bolster PCM composite materials with expanded graphite to improve thermal conductivity while maintaining mechanical flexibility and durability.[14] Additionally, the freedom of material selection and tunability of process parameters with AM can allow for direct integration of PCMs into the device.

Recently, interest has been building in PCM integration with various forms of AM, including filament-based, resin-based, ink-based, and powder-based material processing.[8] These have mainly focused on (1) blending PCMs with AM materials,[15–22] (2) utilizing microencapsulated-PCM (MEPCMs),[13,17,23,24] and (3) chemically grafting PCMs with the AM matrix material[25–28] in efforts to create form-stable, TES composites. Filament-based PCM composite materials and with their properties are reported in **Table 1** and compared with this work. Among these, utilizing commercially available MEPCMs appears to be one of the most accessible pathways to increase energy density by increasing PCM content with minimal risk of PCM leakage from the printed material. Filament-based AM is the most widely used AM technique due to the low cost of materials and equipment. Additionally, for applications outside of AM, developing MEPCM-polymer composite materials that are suited to traditional polymer processing like compression molding or injection molding are also of interest for widespread adoption.

Existing efforts to incorporate large quantities of MEPCMs into AM filaments have been limited by (1) a sufficiently tacky matrix polymer that can cohesively hold large quantities of compounded particles, (2) a sufficiently rigid, yet not brittle composite filament that can be printed at high speeds and resolution, and (3) composite filament extrusion that does not damage the MEPCM.[13,17,23] In this work, it was found that thermoplastic polyurethane (TPU) allowed for large quantities of MEPCM to be compounded into a filament but was excessively soft and difficult to print due to buckling of the filament and abrasion from the geared motors. Simultaneous work utilized polycaprolactone (PCL) and found that similarly large quantities of MEPCM could be compounded into a filament, but the resulting filament was brittle and easily fractured during handling (e.g., manual spooling and pulling through geared motors). Combining both polymers with MEPCM in a powder-based filament extrusion approach balanced the materials properties such that high-volume, high-energy density filaments and prints could be manufactured on commercially available extruders and 3D printers as well as processed through traditional polymer molding techniques. These efforts further both TES devices and AM to demonstrate higher energy densities and higher resolutions than have been previously achieved in the literature (**Table 1**), meaning these composites can be tailor made to integrate into tight operational spaces or retrofit into existing devices to bolster thermal management. This material also maintains mechanical integrity and thermal cyclability, which have not been well characterized in this space were long-lasting solutions are paramount. The innovation in powder material processing and filament extrusion enables use of any polymer-based MEPCM, which have transition temperatures between -10 °C to 70 °C, allowing for diverse TES applications.[29]

Table 1. Comparison of PCM-filament composite composition and properties reported in literature.

References	Filament Polymer	PCM	PCM Loading	Print Size (LxWxH, cm)	Melt Temp. (°C)	Latent Heat (J/g)
Present Study	TPU-PCL	Nextek 6D	60 wt%	10 x 10 x 11.5	6	105
Yang, 2022[28]	TPU	PEG 8000	50 mol%	20 x 20 x 0.4	65	65

Singh, 2021[13]	Nylon	Nextek 6D	30-40 wt%	10 x 10 x 11	6	46
Freeman, 2021[15]	HDPE	Puretemp 42	20-60 wt%	2.5 x 2.5 x 0.4	42	64
Salgado-Pizzaro, 2021[17]	PCL	Rubitherm RT27	10-60 wt%	3.5 x 1.2 x 0.2	27	90
	PCL	Micronal DS5040	10-60 wt%	n/a	22	90
Freeman, 2019[16]	HDPE	Puretemp 42	20-60 wt%	n/a	42	44
Rigotti, 2018[23]	TPU	Nextek 6D	30-60 wt%	n/a	6	70
Freeman, 2018 [30]	HDPE	Puretemp 42	20-60 wt%	n/a	42	44

2 METHODS

2.1 Materials

The PCM composite materials were fabricated from CAPA 6506 PCL powder obtained from Ingevity, TPU powder obtained from STS Inks, and MEPCM with a transition temperature of 6 °C (6D MEPCM), suitable for air-conditioning applications in buildings, obtained from Microtek. The MEPCM is reported to have a composition of 18 wt.% melamine formaldehyde shell and 82 wt.% paraffin wax PCM. Properties of the constituent materials are outlined in **Table 2**.

Table 2. Reported and measured properties of constituent materials.

Material	Manufacturer Reported Average Particle Size (μm)	Measured Melt Temperature (°C)	Measured Latent Heat (J/g)
PCL powder	200–400	50	75.5
TPU powder	20–80	107	n/a
6D MEPCM particles	22.8	6	183

2.2 Material Processing

Initial integration of MEPCM with matrix polymers focused on increasing the MEPCM ratio while maintaining smooth, consistent filament extrusion. For both TPU and PCL, that upper boundary was 60 wt.% MEPCM, above which filament cohesion and printability became an issue. To explore synergy of composite properties, five composite material ratios were produced with 60 wt.% 6D MEPCM, and the other 40 wt.% varied the ratio of TPU to PCL. The notation for the MEPCM composite material ratio is $P_xT_yM_{60}$, where "x" is the weight percent of PCL and "y" is the weight percent of TPU. The weight percent of MEPCM remains constant across the five ratios. Similarly, the polymer-only samples are denoted as P_{100}, $P_{50}T_{50}$, and T_{100} to indicate weight ratios. **Figure 1** outlines the five composite material ratios produced in this work. These five ratios were chosen to understand the effect of the multi-material blending on filament production and printability.

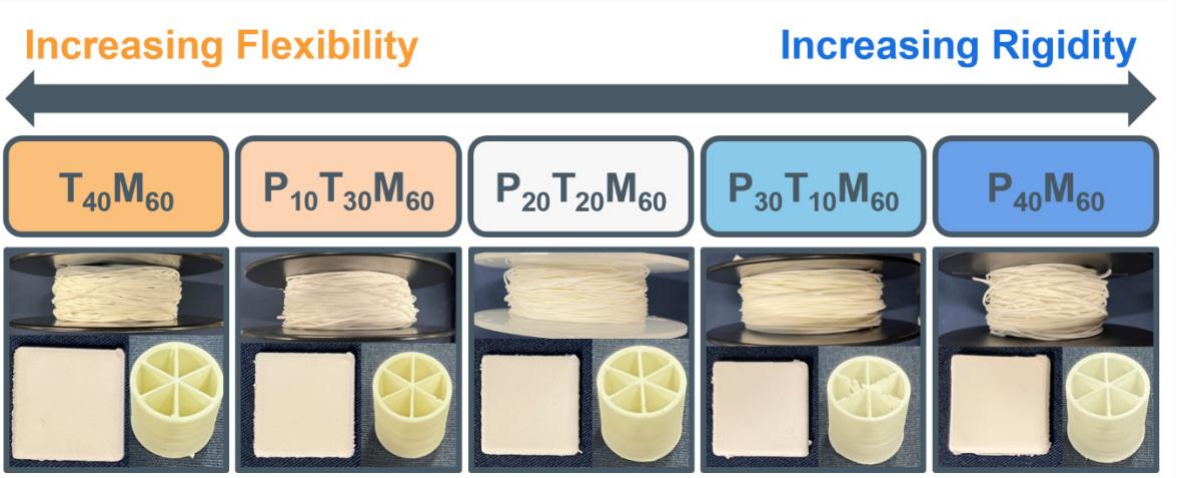

Figure 1. MEPCM composite materials ranging from more flexible (TPU) to more rigid (PCL) at a constant MEPCM ratio of 60 wt.% and 40 wt.% polymer. Each subscript denotes the weight percentage with T – TPU, P – PCL, M – 6D MEPCM. Below each ratio are images of the extruded filament, 100% rectilinear infill test squares (20 mm x 20 mm x 2 mm rectangular prism), and 10% triangle infill cylinder (15 mm diameter, 15 mm tall cylinder) to assess initial print conditions and behaviors of composite materials.

2.2.1 AM Material Processing

MEPCM composite production followed the general scheme shown in **Figure 2,** including three main steps: (1) constituent powder mixing, (2) filament extrusion, and (3) 3D printing. In the first step, polymer powders were mixed with the MEPCM particles and placed on a roller mixer for two days with intermittent shaking. A key factor for success in this method was the use of polymer powder rather than polymer pellets, which are often on the order of several millimeters in size. This is because it was found that polymer pellets tend to damage MEPCM particles as they are mechanically sheared through a screw-based extrusion and require multiple rounds of extrusion due to separation of pellets from powders. Using powders allows for improved homogeneity of mixed material, rapid polymer melting, and minimized damage to the MEPCM shells. Extrusion was done on a 3devo Precision 350 single screw extruder with a 4-stage temperature profile from hopper to nozzle of 135 °C, 150 °C, 160 °C, and 150 °C, screw speeds between 3 and 5 RPM, and through a 1.80 mm nozzle. Printing parameters and optimization were completed on a Hyrel ESR using a combination of SuperSlicer and Slic3r. In orienting samples specifically for mechanical testing, the x-direction indicates along the filament axis, y-direction is orthogonal to the filament but within the same layer, and z-direction is in the direction of additional layer deposition also the vertical build direction. Tensile samples (Type IV dogbones) were printed using the high-resolution settings from **Table 3** with a 100% rectilinear infill pattern. The x-print samples were printed flat on the bed to ensure filament alignment in the necked region and z-print samples were printed upright to ensure the necked region was only relying on interlayer adhesion. No supports or post processing was used for any tensile samples. During printing of other objects, variable infill geometries and percentages were utilized to test the capabilities of this materials including: rectilinear (100%), concentric (100%), gyroid (15-50%), and honeycomb (30%) with specific printing parameters outlined in **Table 3**.

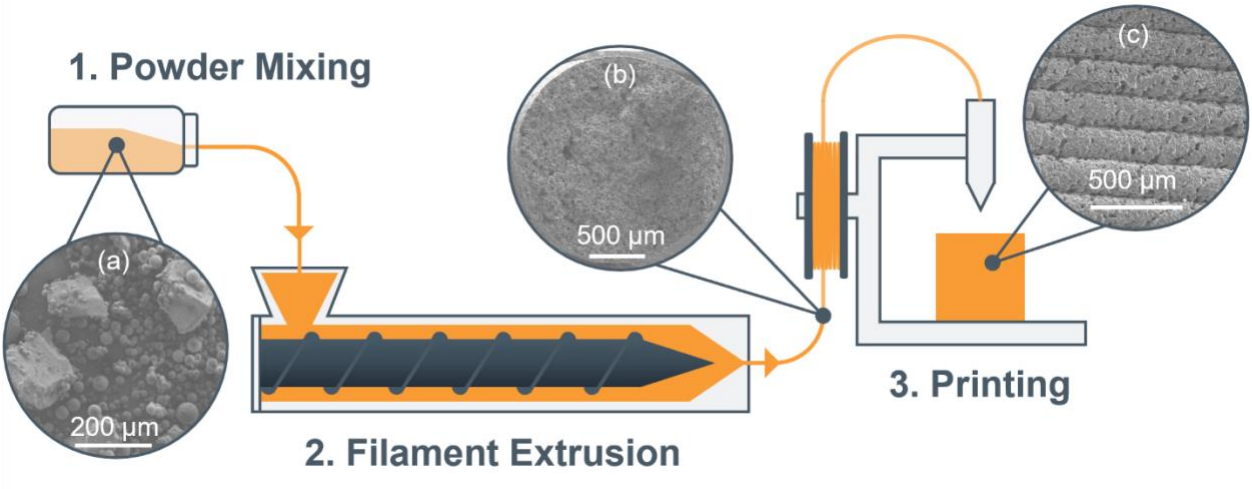

Figure 2. Processing schematic for MEPCM composite materials from powdered state to printed parts with scanning electron microscopy images (a) $P_{20}T_{20}M_{60}$ powder, (b) $P_{20}T_{20}M_{60}$ filament, and (c) $P_{20}T_{20}M_{60}$ print.

Table 3. Typical printing parameters for MEPCM composite filaments under two conditions.

Parameter	High-Resolution	High-Volume
Nozzle diameter	0.4 mm	0.8 mm
Extrusion temperature	200 °C	200 °C
Bed temperature	40 °C	40 °C
Layer height	0.2 mm	0.3 mm
Layer width	0.50–0.55 mm	0.90–0.95 mm
Extrusion multiplier	1.00–1.05	1.00
Print speed	15 mm/s	15 mm/s

2.2.2 Molded Materials Processing

Molding composites was done in a couple of ways depending on the state of the material and included (1) compression molding, (2) injection molding, and (3) open molding. Compression-molded MEPCM composite samples were produced to compare thermal conductivity and hardness with printed composites. Compression molding was done in a 2-inch steel die press preheated to 200 °C, where about 5 mm of compounded material was added and allowed to melt over 20 minutes. Manual hand pressing of the die press ensured full consolidation of the material. The die press was allowed to cool down to room temperature before demolding the sample to prevent deformation. Injection molding was used to make the MEPCM composite tensile specimens and was done on a Pim-Shooter Model 150A (LNS Technologies, Scotts Valley, California) with a barrel temperature between 135 °C and 180 °C and an oven temperature of 120 °C. Open molding was used to make pure polymer tensile specimens for mechanical testing because injection molding was not successful for these materials. A Teflon mold milled for type IV tensile specimens was preheated to 200 °C, followed by sequential addition of thin layers of polymer powder every 10 minutes to allow for full melting and consolidation in the mold until full (around 6 rounds of powder addition) before slow cooling in the oven.

2.3 Material Properties Characterization

The thermal energy storage ability of the MEPCM composite materials was measured with a TA DSC 2500 differential scanning calorimeter (DSC) in a nitrogen atmosphere (50 mL/min) with a ramp rate of 5 °C/min across a temperature range of -50 °C to 100 °C. Thermal conductivity was measured on a TA DTC 300 guarded heat flow meter at a set point of 25 °C. Thermal stability was measured using a TA TGA Q500 thermogravimetric analyzer (TGA), in a nitrogen atmosphere (60 mL/min) with a ramp rate of 5 °C/min up to 800 °C. Imaging of samples was completed using a Hitachi 4800 scanning electron microscopy (SEM). Samples were coated in platinum and images were collected with an acceleration voltage of 5.0–10.0 kV. Image analysis was conducted using ImageJ software. Tensile testing was completed on an Instron 5966 with a 10-kN load cell using a strain rate of 5 mm/min, in accordance with ASTM D638-14. Five tensile samples were tested to ensure representative data, except for $T_{40}M_{60}$ printed in the z-direction, where only three samples could be produced. Hardness testing was done using an analog VTSYIQI Shore D Durometer, sampling 10 spots on each material for representative data.

3 RESULTS AND DISCUSSION

3.1 Material Production and Additive Manufacturing

Figure 3a–c shows SEM images of the raw materials prior to powder mixing and filament processing as well as the extruded filaments of MEPCM composites in **Figure 3d–f**. The PCL and TPU powders are simply shredded polymers with a wide range of particle sizes from tens of microns to several hundreds of microns. 6D MEPCM is smaller than both polymers with a listed d_{50} = 20 μm with a broad spread of particle sizes. With the polymer powder particles on this size scale, the MEPCM was well incorporated and extruded into filament. Using traditional polymer pellets, the mixing of materials was less homogeneous and resulted in crushed MEPCM and pooling PCM liquid in the extruder (data not shown). The filaments in **Figure 3d–f** do not appear different across material ranges and show the high packing density of MEPCM and minimal void space within the cross section. While the filaments were not visually distinct, there were dramatic differences in the flexibility of the filaments. $P_{40}M_{60}$, which was the stiffest material, would occasionally break in a brittle manner when handled due to the high MEPCM content, while $T_{40}M_{60}$ remained comparatively soft and flexible even at the high MEPCM loadings. Any amount of TPU ($P_{30}T_{10}M_{60}$, $P_{20}T_{20}M_{60}$, and $P_{10}T_{30}M_{60}$) in the filament mitigated breakage of the filaments.

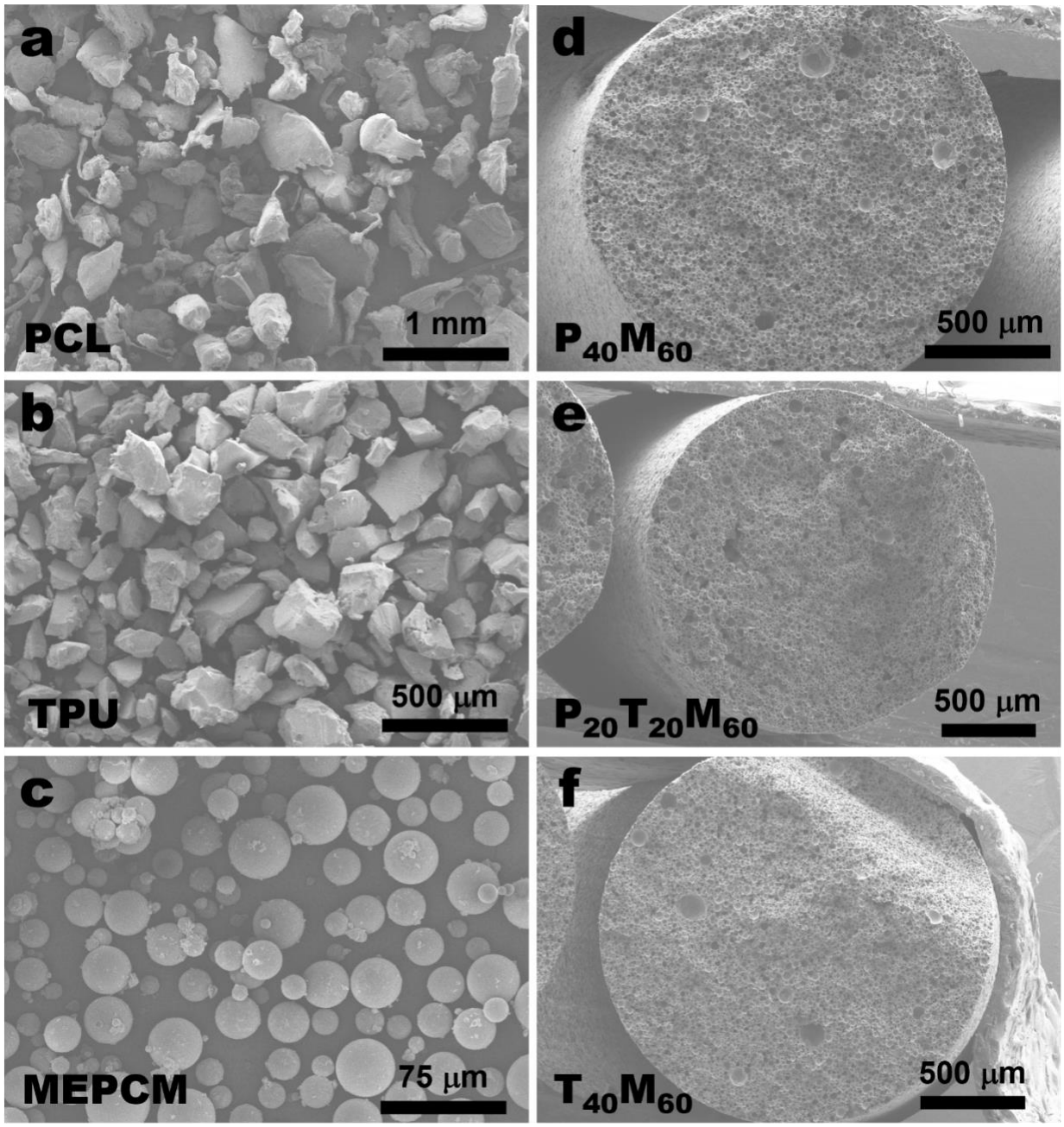

Figure 3. SEM micrographs for the raw materials (a–c) and selected extruded filament freeze fractured cross sections (d–f). (a) PCL powder, (b) TPU powder, and (c) 6D MEPCM powder were mixed and extruded into filaments (d) $P_{40}M_{60}$, (e) $P_{20}T_{20}M_{60}$, and (f) $T_{40}M_{60}$.

Initial integration of PCL and TPU found that they compounded well together in the filament form and the differential melt/flow temperature between the two polymers (TPU: 107 °C and PCL: 50 °C) was helpful in achieving good layer adhesion during printing. Test prints, shown in **Figure 1**, were made with the MEPCM composite filaments to optimize the printing parameters to suit both 100% infill and thin-walled structures. Building on this initial optimization, both high-resolution and high-volume methods are outlined in **Table 3** to both compete with commercial AM material parameters and emphasize a higher

material throughput method for an eye toward scalability. During AM, there was some difficulty with printing $T_{40}M_{60}$ on a direct drive printer because the softness of the TPU-rich material could easily kink and get damaged by the gear of the drive motor, causing prints to fail. With any amount of PCL ($P_{10}T_{30}M_{60}$, $P_{20}T_{20}M_{60}$, and $P_{30}T_{10}M_{60}$), there was enough rigidity to mitigate the issues with printing on a direct drive printer.

Prints of these composite materials using the high-resolution settings were examined with an SEM to provide insights into material behaviors and small-scale print quality. At the surface level of tensile specimens in **Figure 4a–c,** there are evident print quality differences between the PCL-rich and TPU-rich materials. For $P_{40}M_{60}$ and $P_{20}T_{20}M_{60}$, the exterior shows a smoother surface compared with the $T_{40}M_{60}$ print. This could be a result of the lower melting temperature of the PCL effectively annealing at the surface to form smoother textures. When looking at the fractured cross sections from tensile testing, however, layers of the $P_{40}M_{60}$ in **Figure 4d** resisted internal flow that would fill in gaps formed by joining rounded layers as shown by the void space surrounding each pass of the printer nozzle. In **Figure 4e,** the cross-section edge of the $P_{20}T_{20}M_{60}$ print shows each individual layer bulging outwards, but the interior is well-filled with nearly no void space, indicating that the layer deposition exhibited better void filling. The individual layers of the $P_{20}T_{20}M_{60}$ were nearly indistinguishable. In the $T_{40}M_{60}$ cross section, there is less void space compared to $P_{40}M_{60}$ within each layer indicating that there was good melding of adjacent lines, but there are distinct layer lines in the vertical direction. Analysis of these images to quantify the void space revealed that the $P_{40}M_{60}$ print was 3.2% voids, $P_{20}T_{20}M_{60}$ was 0.7% voids, and $T_{40}M_{60}$ was 1.2% void space. The benefits of both PCL and TPU in the $P_{20}T_{20}M_{60}$ composite print appear to improve the internal structure with increased space filling of layers and greater interfacial homogeneity across layers.

With the optimized print parameters in place, a variety of geometries and infill ratios were produced. **Figure 5** contains numerous types of AM pieces along with a compression-molded puck to demonstrate alternative manufacturing techniques. This suite of objects was selected to test the composites' capability to produce 100% infilled (solid) objects as well as complicated, high surface area geometries toward more efficient heat transfer. **Figure 5e** shows a 15% gyroid infill, a complicated open-cell geometry that requires the filament to be able to bridge between segments. The 50% gyroid cube in **Figure 5f** was demonstrated to be watertight over the course of 1 week with no observed leakage. Based on the results from extrusions and prints, $P_{20}T_{20}M_{60}$ demonstrated the greatest reliability and was the material of primary interest that was more extensively tested than other material ratios along with testing larger scale prints like the 900 cm^3 honeycomb infill heat exchanger shown in **Figure 6**.

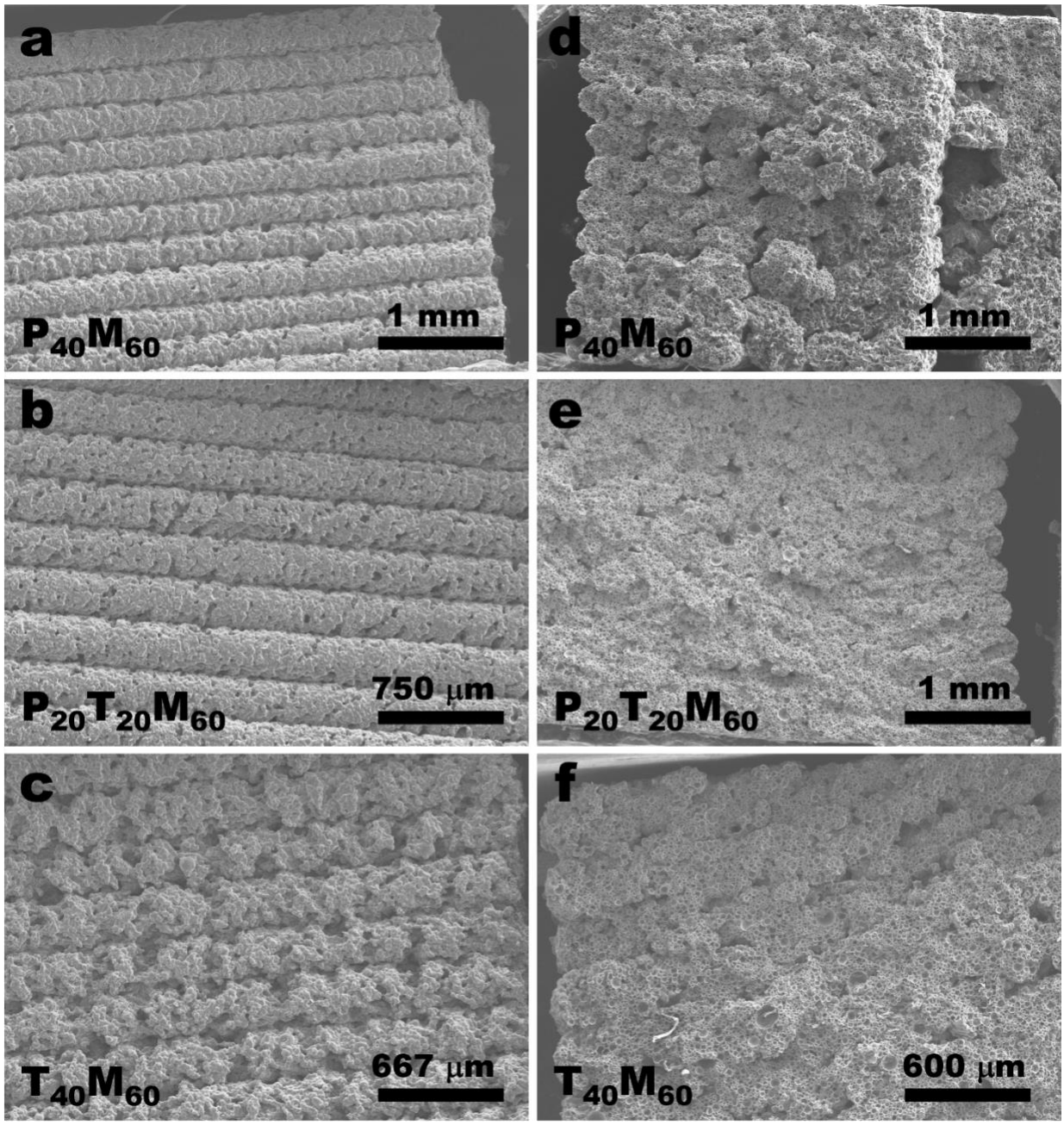

Figure 4. SEM micrographs of tensile specimens printed in the x-direction showing the side views (a–c) and cross sections (d–f) for (a, d) $P_{40}M_{60}$, (b, e) $P_{20}T_{20}M_{60}$, and (c, f) $T_{40}M_{60}$.

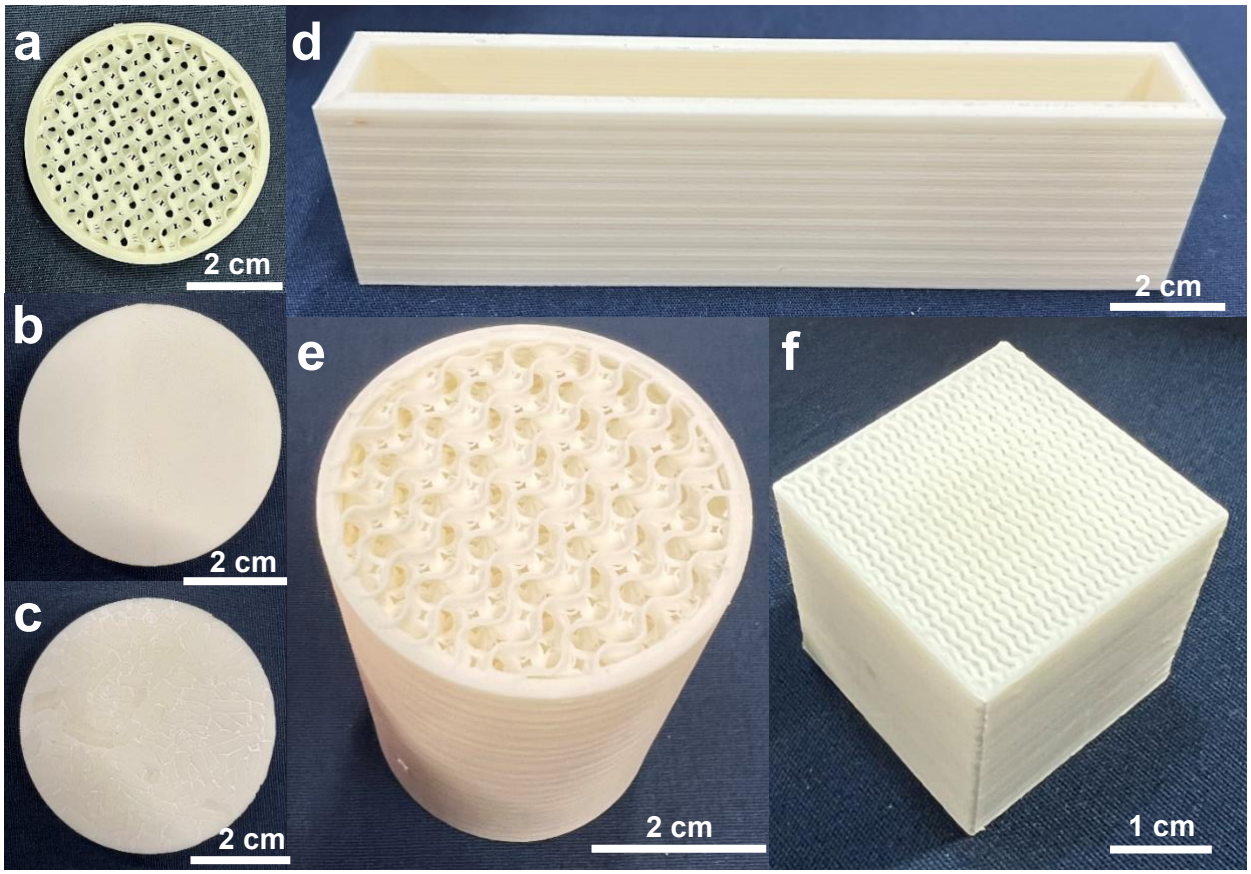

Figure 5. Variety of manufactured parts, including (a) 15% gyroid infill scaffold cross section made from $P_{20}T_{20}M_{60}$, (b) 100% concentric infill printed puck made from $P_{20}T_{20}M_{60}$, (c) molded puck made from $T_{40}M_{60}$, (d) rectangular perimeter scaffold made from $T_{40}M_{60}$, (e) 15% gyroid infill scaffold from $P_{20}T_{20}M_{60}$, and (f) 50% gyroid infill cubic scaffold from $P_{20}T_{20}M_{60}$.

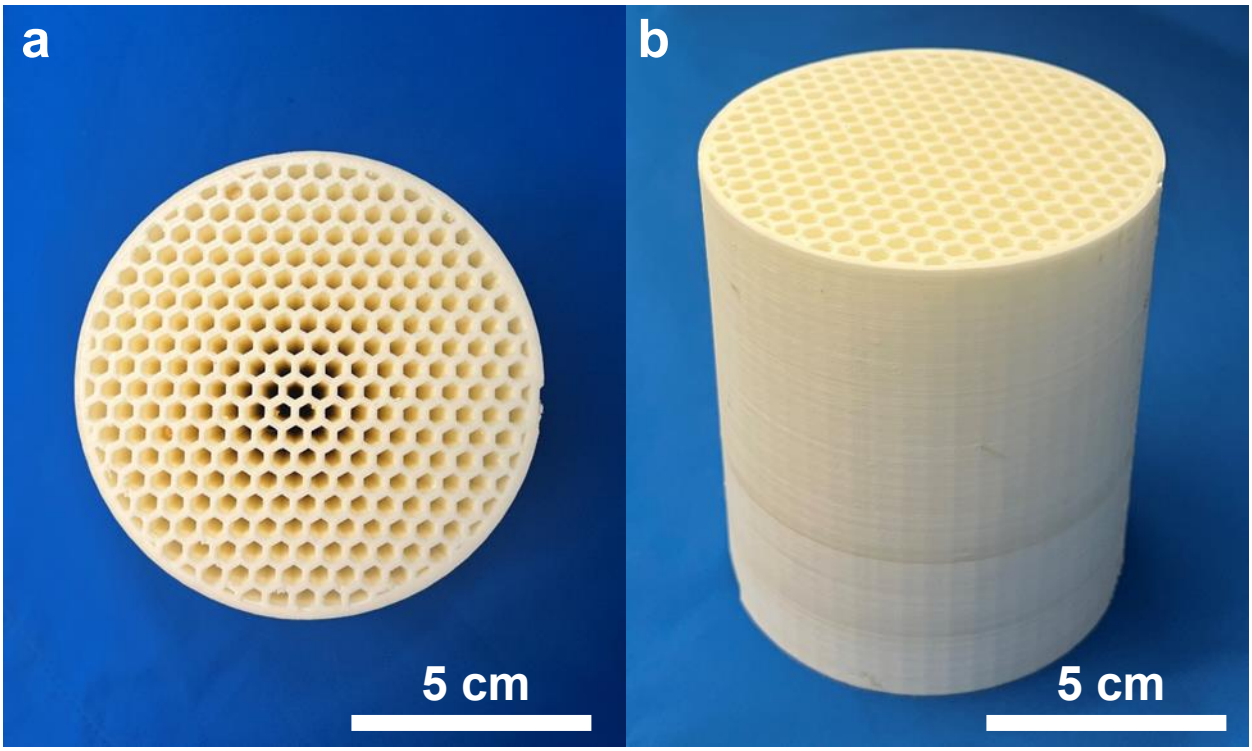

Figure 6. High volume print with 30% honeycomb infill made from $P_{20}T_{20}M_{60}$ that has a diameter of 10 cm and height of 11.5 cm. This printed TES composite has an energy storage capacity around 9 Wh.

3.2 Thermal Properties

Thermal properties discussed here are separated into (1) enthalpies of phase transition, (2) thermal stability, and (3) thermal conductivities.

As a result of the multiple processing steps, from mixing constituent powders to compounding *via* melt extrusion to AM, mechanical forces and high temperature exposure can impart damage to the MEPCM shells. This damage leads to leakage of paraffin PCM from shells, possible evaporation at elevated processing temperatures, and an overall reduction in transition enthalpy for the composite. To ensure retention of TES properties, latent heats of transition were measured for the mixed powders, extruded filaments, and printed objects for each material and are shown in **Figure 7a** with a dashed line denoting the theoretical transition enthalpy for 60 wt.% of the 6D MEPCM at 109.8 J/g (pure 6D MEPCM = 183 J/g). Except for the printed $P_{40}M_{60}$, each of the materials averaged over 100 J/g with minimal to no deterioration in transition enthalpy, meaning the powder processing method presented here is a robust means to integrate MEPCM into filament materials. Additionally, the printed $P_{20}T_{20}M_{60}$ was subjected to 250 thermal cycles on the DSC in **Figure 7b** with no substantial difference in melt behavior for the MEPCM, maintaining a $T_{m,onset}$ of 3.3°C, $T_{m,peak}$ of 8.6°C, and a $\Delta H_{m,MEPCM}$ of 103.5 J/g, indicating fidelity of the MEPCM shells. Shell damage and subsequent leakage tends to shift the transition temperature due to changes in heat transfer and nucleation through the sample. Apart from subtle changes in peak shape on crystallization, the only difference in melt/freeze behavior is between the first PCL melt cycle and subsequent PCL melt cycles. PCL, being a semicrystalline polymer, has observable melting and crystallization peaks around 52°C and 25°C, respectively. With immediate cycling of PCL, there is a shift in peak location and magnitude between the first melt cycle and subsequent melt cycles, which afterward appear identical. This is a result of the kinetics of PCL crystallization, where further crystallization occurs at room temperature over a longer period. See **Figure S1**, which shows the same PCL-MEPCM sample

cycled three times then again after one week. In each set of cycles, the first cycle is higher in both temperature and enthalpy showing deviations after the first cycle in each case.

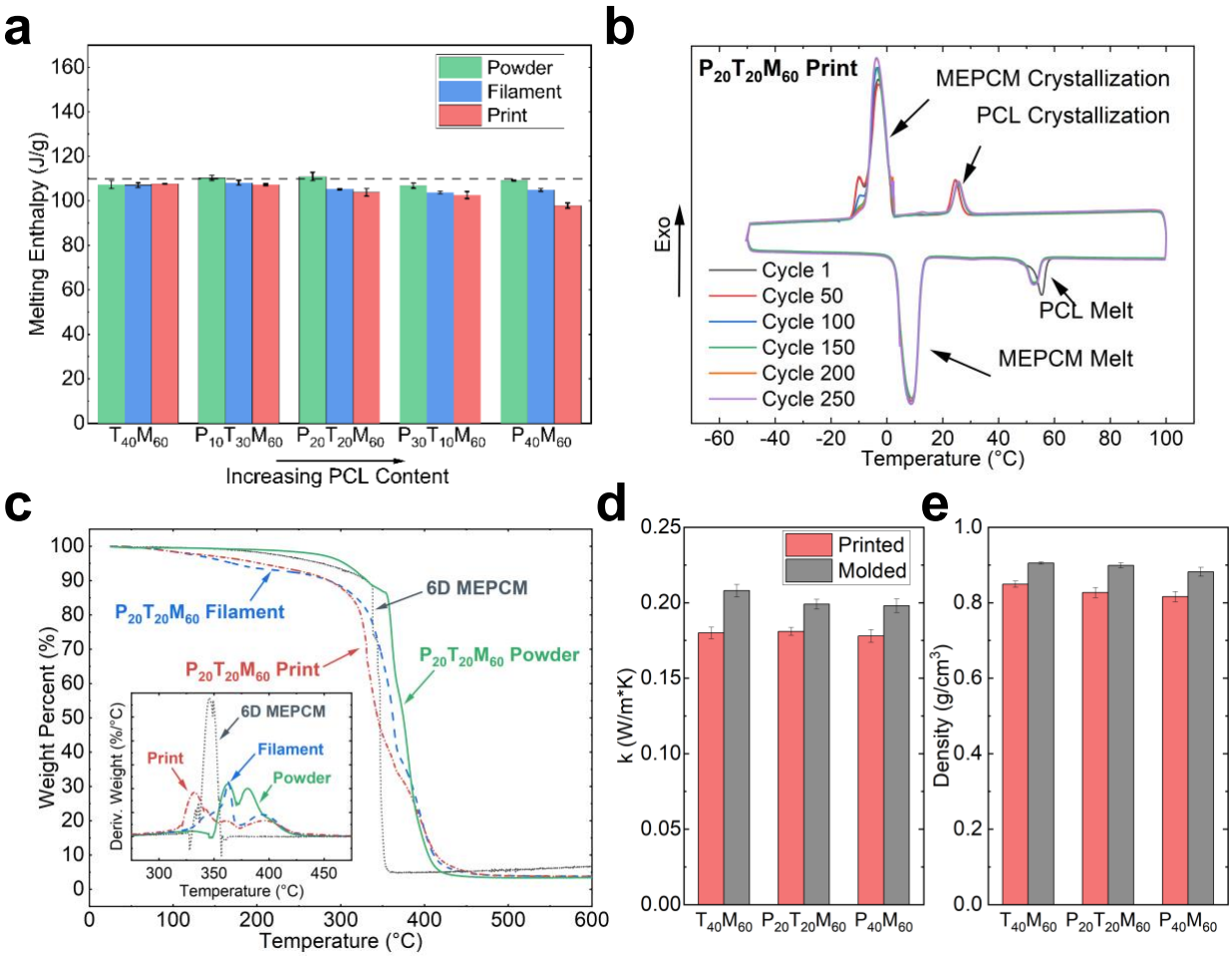

Figure 7. (a) Melting enthalpies of MEPCM composite materials in powder, filament, and print states. Dashed line represents the theoretical enthalpy of 109.8 J/g based on 60 wt.% of the latent heat of 6D MEPCM (183 J/g). (b) DSC thermogram showing 250 thermal cycles of a $P_{20}T_{20}M_{60}$ print. (c) TGA traces showing the thermal decomposition of pure MEPCM powder and $P_{20}T_{20}M_{60}$ powder, filament, and print with the first derivative curves shown in an inset plot. (d) Thermal conductivities and (e) densities comparing molded and printed samples of $T_{40}M_{60}$, $P_{20}T_{20}M_{60}$, and $P_{40}M_{60}$.

Figure 7c shows representative TGA decomposition curves for $P_{20}T_{20}M_{60}$ in powder, filament, and print states compared with decomposition of pure MEPCM with first derivative as an inset plot. 6D MEPCM alone exhibits a rapid decomposition at 347°C due to the stability of the shell material compared to the paraffin core. TGA is a useful tool to assess MEPCM damage that would lead to the PCM leaking from the shell because of the lower volatilization temperature of the PCM compared to the shell materials. **Figure S2a** shows the paraffin volatilization around 150°C after acetone treatment of MEPCM that caused paraffin to be extracted from the shell. Comparing $P_{20}T_{20}M_{60}$ in each of its states, there is minimal difference in the decomposition profiles of mixed powder, extruded filament, and printed material, with onset decomposition occurring at 320°C and 350°C. This means that the materials are stable well within the processing temperatures for these materials and indicates that the overwhelming majority of MEPCM

remains intact throughout the various mechanical and thermal processing steps. Additional decomposition curves can be found in **Figure S2** for all constituents, mixed powders, filaments, and prints.

Comparisons of thermal conductivity and density between printed (100% infill **Figure 5b**) and molded (**Figure 5c**) samples of $T_{40}M_{60}$, $P_{20}T_{20}M_{60}$, and $P_{40}M_{60}$ are shown in **Figure 7d** and were taken at 25°C. Despite both samples being the maximum densities for their respective manufacturing methods, it was expected that both thermal conductivities and densities of the molded pucks would be slightly higher than printed pucks because of the abundance of layer interfaces and possible voids resulting from AM processing. Thermal conductivities were broadly in the range of 0.18–0.21 W/m·K for all materials, with an approximate 9%–13% drop in conductivity from molded to printed materials. While all AM materials had conductivities within error of each other, molded $T_{40}M_{60}$ was slightly more conductive and more dense than molded $P_{40}M_{60}$. The lowered conductivity is likely due to the crystallization of the PCL pulling away from the MEPCM and creating small interfacial gaps that contribute to lower heat transfer. Thermal conductivities are an important component to efficient charging and discharging of the PCM; however, with AM, decreased length scales and increased surface area can be achieved to increase heat transfer to and from the PCM, reducing the need for very high thermal conductivity.

3.3 Mechanical Properties

Tensile properties were tested on an Instron to assess the molded and printed properties of two orientations of these materials and are shown in **Figure 8**. Notably, injection molding was used for the MEPCM composite materials due to the inability of tensile specimens to be effectively open molded in an oven, while polymer-only samples were open molded in an oven due to their inability to be injection molded. Injection molding serves to demonstrate an alternative manufacturing technique applicable to these composites outside of AM, though with reduced feature resolution. The need for MEPCM composites to undergo extrusion or injection molding suggests that external forces are required to form tightly packed homogenous materials. It was expected that the printed materials would exhibit highly anisotropic behavior comparing the properties of aligned filaments (x-direction) with interlayer adhesion (z-direction). PCL primarily contributed to the strength and stiffness of composites, whereas TPU increased the elasticity of the composites. Maximum stress and elastic modulus for molded samples were higher than that of printed samples, which was expected for the bulk material (**Figure 8a-b**). With average percent elongation, however, the molded samples were comparable to or lower than the printed samples, except for $T_{40}M_{60}$ printed in the z-direction, which had a smaller elongation compared to the other $T_{40}M_{60}$ samples (**Figure 8c**). In most cases for printed composites, there were little to no differences in maximum stress between the x-direction and the z-direction.

The decrease in maximum stress between molded and printed $P_{20}T_{20}M_{20}$ (15%–20%) was smaller than that of the $P_{40}M_{60}$ and $T_{40}M_{60}$, which were in the range of a 27%–35% decrease. However, the maximum stress of $P_{40}M_{60}$ and $T_{40}M_{60}$ in the x- and z-directions were within the error of each other, indicating that the printing process yielded strong interlayer adhesion. Elastic moduli generally followed the trend of molded > x-direction > z-direction, except for $T_{40}M_{60}$, which had a higher z-direction modulus than x-direction modulus. The lower elastic modulus for the $T_{40}M_{60}$ in the x-direction could be a result of the rougher, fragmented surface shown in **Figure 4c**, which may have contained flaw sizes that allowed the material to yield and stretch at lower stresses. $P_{20}T_{20}M_{60}$ exhibited a 20% decrease in elastic modulus between the molded and x-direction samples, where the stiffness decrease was about 30% for $P_{40}M_{60}$ and $T_{40}M_{60}$. Notably, the percent elongation at break for molded composites was lower or within error of the x-direction samples. The z-direction printed samples had elongations lower than the x-direction, which was expected due to anisotropy in layered composites. In the case of the $P_{20}T_{20}M_{60}$ composites, the molded and z-direction samples had elongations that were within the error of each other, suggesting good interlayer adhesion with printing. Comparison of tensile properties with the constituent polymers is

difficult given that the behavior of the composites relative to the polymers was dramatically different. Using ASTM D638-14 at the strain rate of 5 mm/min, T_{100} and $P_{50}T_{50}$ did not exhibit rupture, yield, or reach a maximum stress within the 0.5–5 min time scale, whereas all other composites ruptured within that timeframe. Only P_{100} yielded within this test at an average maximum stress of 18.6 ± 0.3 MPa, which was double that of the molded $P_{40}M_{60}$ and triple that of the printed $P_{40}M_{60}$. The elastic moduli of P_{100}, $P_{50}T_{50}$, and T_{100} were 513.8 ± 3.3 MPa, 150.2 ± 4.6 MPa, and 18.9 ± 0.7 MPa, respectively. Only T_{100} had a comparable elastic modulus to the molded composite, $T_{40}M_{60}$; all other composites were considerably reduced.

Additionally, hardness testing was performed to see the comparative differences among polymers, the effect of MEPCM addition, and the effect of printing. As seen in **Figure 8e**, P_{100} had a hardness value of 51.8, which was more than twice that of the T_{100} at 25.0, and $P_{50}T_{50}$ was in between at 39.0. With MEPCM addition, $P_{40}M_{60}$ and $P_{20}T_{20}M_{60}$ decreased in hardness compared to the polymer-only analogues because PCL is the primary contributor to hardness. For the TPU system, MEPCM addition slightly increased the hardness of $T_{40}M_{60}$ compared to T_{100}. Among MEPCM composites, molded MEPCM composites had slightly larger hardness values than printed samples, likely due to the increased surface roughness and lower density of the printed material compared to the bulk material.

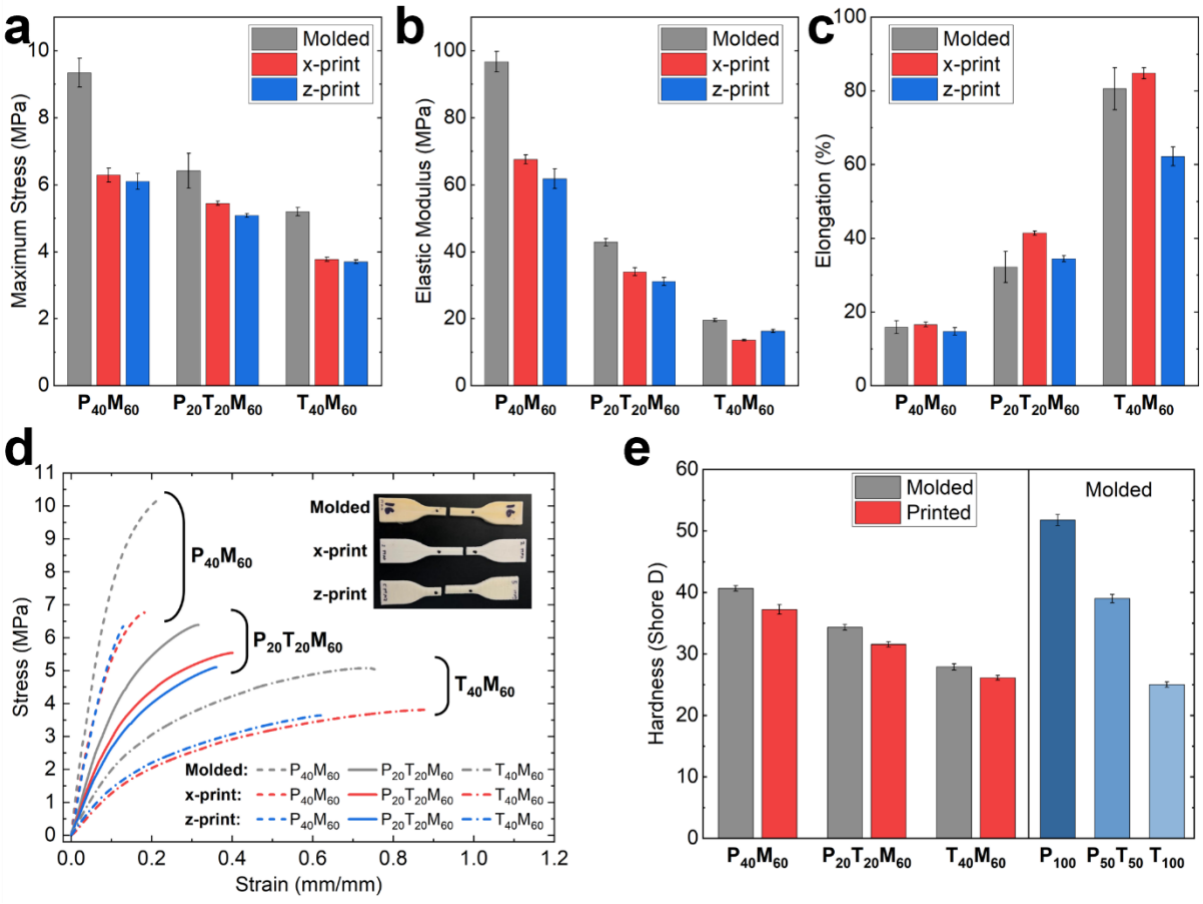

Figure 8. Tensile properties for MEPCM composites that are molded (gray), printed in the x-direction with filaments axially aligned (red), and printed in the z-direction with filaments orthogonal to the tensile axis (blue); (a) maximum stress at fracture, (b) elastic modulus, (c) percentage elongation at fracture, (d)

representative stress strain curves for each material type with an inset image of representative tensile specimens for each $P_{20}T_{20}M_{60}$ sample type, and (e) Shore D hardness for the molded and printed MEPCM composites along with the molded polymers. Note for $T_{40}M_{60}$ z-direction, only 3x tensile specimens could be produced and tested.

4 CONCLUSIONS

Development of form-stable TES materials that can be additively manufactured into thermal management devices has been limited by the quantity of PCM that can be incorporated into the material without deterioration of the PCM or filament properties. In this work, a composite filament was developed containing 60 wt.% MEPCM using two polymers (TPU and PCL) that served to mediate the flexibility and rigidity of the filament such that it can be effectively extruded and printed. Using both polymers in the filament extrusion produced a smooth, stable, consistent filament that was more resilient when printing than the composites made from the individual polymers and MEPCM. The powder-based extrusion process was tailored to have a negligible effect on the MEPCM, remaining undamaged through the printing process to consistently demonstrate 105 J/g of energy storage after 250 thermal cycles. Each of the TES composites produced was within 5% of the theoretical storage enthalpy based on the 60 wt.% loading of MEPCM. The materials produced here can be used on commercially available 3D printers using standard print settings to form complex, high surface area geometries. This was demonstrated by producing both sparse 15% gyroid infills along with solid 100% infill objects. The primary limitation with this work is in the diversity of available powdered polymers for filament production, which can be difficult to manufacture at scale for softer materials. An additional limitation is in material throughput as mixing powders, filament extrusion, and printing are time-intensive processes, especially at high volumetric outputs. Moving toward an application space, a heat exchanger model was produced using the $P_{20}T_{20}M_{60}$ composite material which has an estimated energy storage capacity of 9 Wh. From this work, insights and methods emerged to dramatically increase the ability to produce TES composite filament and prints with higher MEPCM loadings, higher transition enthalpies, and higher material integrity than those achieved in the literature. Additionally, this manufacturing process can be directly translated to other MEPCM transition temperatures to suit other applications. Future work that would benefit this field includes (1) incorporation of soft, non-damaging thermal conductivity enhancers to increase the charge/discharge rates of devices, (2) improved production of powdered polymers to increase the diversity of materials that can be used, and (3) direct powder extrusion printing of the material, bypassing the filament step.

ACKNOWLEDGEMENTS

This work was co-authored by the National Renewable Energy Laboratory, operated by Alliance for Sustainable Energy, LLC, for the U.S. Department of Energy (DOE) under Contract No. DE-AC36-08GO28308. Funding provided by the U.S. Department of Energy Office of Energy Efficiency and Renewable Energy Building Technologies Office and the Advanced Manufacturing Office. The views expressed in the article do not necessarily represent the views of the DOE or the U.S. Government. The U.S. Government retains and the publisher, by accepting the article for publication, acknowledges that the U.S. Government retains a nonexclusive, paid-up, irrevocable, worldwide license to publish or reproduce the published form of this work, or allow others to do so, for U.S. Government purposes.

CONFLICT OF INTEREST

The authors declare no conflict of interest.

REFERENCES

1. Chapter 5: Increasing Efficiency of Building Systems and Technologies. In: Quadrennial Technology Review: An Assessment of Energy Technologies and Research Opportunities. US Department of Energy; 2015.

2. Odukomaiya A, Woods J, James N, Kaur S, Gluesenkamp KR, Kumar N, et al. Addressing energy storage needs at lower cost via on-site thermal energy storage in buildings. Energy & Environmental Science 2021;14(10):5315–29.

3. Yang T, King WP, Miljkovic N. Phase change material-based thermal energy storage. Cell Reports Physical Science 2021;2(8):100540.

4. Hirano S. Thermal Energy Storage and Transport. In: Lackner M, Sajjadi B, Chen WY, editors. Handbook of Climate Change Mitigation and Adaptation. Cham: Springer International Publishing; 2022. page 497–530.

5. Akeiber H, Nejat P, Majid MZAbd, Wahid MA, Jomehzadeh F, Zeynali Famileh I, et al. A review on phase change material (PCM) for sustainable passive cooling in building envelopes. Renewable and Sustainable Energy Reviews 2016;60:1470–97.

6. Paranjothi G, Odukomaiya A, Cui S, Bulk A. Evaluation of phase change plaster/paste composites for building envelopes. Energy and Buildings 2021;253:111372.

7. Arumugam P, Ramalingam V, Vellaichamy P. Effective PCM, insulation, natural and/or night ventilation techniques to enhance the thermal performance of buildings located in various climates – A review. Energy and Buildings 2022;258:111840.

8. Freeman TB, Foster KEO, Troxler CJ, Irvin CW, Aday A, Boetcher SKS, et al. Advanced Materials and Additive Manufacturing for Phase Change Thermal Energy Storage and Management: A Review. Adv Energy Mater 2023;

9. Akhmetov B, Georgiev AG, Kaltayev A, Dzhomartov AA, Popov R. Thermal energy storage systems – review.

10. Al-Abidi AA, Bin Mat S, Sopian K, Sulaiman MY, Lim CH, Th A. Review of thermal energy storage for air conditioning systems. Renewable and Sustainable Energy Reviews 2012;16(8):5802–19.

11. Ben Romdhane S, Amamou A, Ben Khalifa R, Saïd NM, Younsi Z, Jemni A. A review on thermal energy storage using phase change materials in passive building applications. Journal of Building Engineering 2020;32:101563.

12. Goyal A, Kozubal E, Woods J, Nofal M, Al-Hallaj S. Design and performance evaluation of a dual-circuit thermal energy storage module for air conditioners. Applied Energy 2021;292:116843.

13. Singh P, Odukomaiya A, Smith MK, Aday A, Cui S, Mahvi A. Processing of phase change materials by fused deposition modeling: Toward efficient thermal energy storage designs. Journal of Energy Storage 2022;55:105581.

14. Huang Y, Zou M, Chen W, Luo W, Hu X, Zhu G, et al. A Novel Room-Temperature Flexible Phase Change Material for Solar Energy Photothermal Conversion and Battery Thermal Management. ACS Sustainable Chem Eng 2024;12(11):4662–75.

15. Freeman TB, Messenger MA, Troxler CJ, Nawaz K, Rodriguez RM, Boetcher SKS. Fused filament fabrication of novel phase-change material functional composites. Additive Manufacturing 2021;39:101839.

16. Freeman TB, Spitzer D, Currier PN, Rollin V, Boetcher SKS. Phase-Change Materials/HDPE Composite Filament: A First Step Toward Use With 3D Printing for Thermal Management Applications. Journal of Thermal Science and Engineering Applications 2019;11(5):054502.

17. Salgado-Pizarro R, Padilla JA, Xuriguera E, Barreneche C, Fernández AI. Novel Shape-Stabilized Phase Change Material with Cascade Character: Synthesis, Performance and Shaping Evaluation. Energies 2021;14(9):2621.

18. Wei P, Cipriani CE, Pentzer EB. Thermal energy regulation with 3D printed polymer-phase change material composites. Matter 2021;4(6):1975–89.

19. Wang C, Liu C. Additive Manufacturing of Shape-Stabilized Composite Phase Change Materials Via Ultraviolet Curing. SSRN Journal [Internet] 2022 [cited 2022 Aug 26];Available from: https://www.ssrn.com/abstract=4173655

20. Nofal M. Experimental investigation of phase change materials fabricated using selective laser sintering additive manufacturing. Journal of Manufacturing Processes 2019;44:91–101.

21. Nofal M, Pan Y, Al-Hallaj S. Selective Laser Sintering of Phase Change Materials for Thermal Energy Storage Applications. Procedia Manufacturing 2017;10:851–65.

22. Nofal M, Al-Hallaj S, Pan Y. Thermal management of lithium-ion battery cells using 3D printed phase change composites. Applied Thermal Engineering 2020;171:115126.

23. Rigotti D, Dorigato A, Pegoretti A. 3D printable thermoplastic polyurethane blends with thermal energy storage/release capabilities. Materials Today Communications 2018;15:228–35.

24. Cui H, Yu S, Cao X, Yang H. Evaluation of Printability and Thermal Properties of 3D Printed Concrete Mixed with Phase Change Materials. Energies 2022;15(1978).

25. Ma J. 3D Printable, Recyclable and Adjustable Comb/Bottlebrush Phase Change Polysiloxane Networks toward Sustainable Thermal Energy Storage. Energy Storage MaterialsJ Ma 2021;39:294–304.

26. Ma J, Ma T, Cheng J, Zhang J. Polymer Encapsulation Strategy toward 3D Printable, Sustainable, and Reliable Form-Stable Phase Change Materials for Advanced Thermal Energy Storage. ACS Appl Mater Interfaces 2022;14(3):4251–64.

27. Mao Y, Miyazaki T, Sakai K, Gong J, Zhu M, Ito H. A 3D Printable Thermal Energy Storage Crystalline Gel Using Mask-Projection Stereolithography. Polymers 2018;10(10):1117.

28. Yang Z, Ma Y, Jia S, Zhang C, Li P, Zhang Y, et al. 3D-Printed Flexible Phase-Change Nonwoven Fabrics toward Multifunctional Clothing. ACS Appl Mater Interfaces 2022;14(5):7283–91.

29. Sheikh Y, Hamdan MO, Sakhi S. A review on micro-encapsulated phase change materials (EPCM) used for thermal management and energy storage systems: Fundamentals, materials, synthesis and applications. Journal of Energy Storage 2023;72:108472.

30. Freeman TB, Nabutola K, Spitzer D, Currier PN, Boetcher SKS. 3D-Printed PCM/HDPE Composites for Battery Thermal Management. In: Volume 8B: Heat Transfer and Thermal Engineering. Pittsburgh, Pennsylvania, USA: American Society of Mechanical Engineers; 2018.